The SALTENA Experiment: Comprehensive Observations of Aerosol Sources, Formation, and Processes in the South American Andes

Federico Bianchi, Victoria A. Sinclair, Diego Aliaga, Qiaozhi Zha, Wiebke Scholz, Cheng Wu, Liine Heikkinen, Rob Modini, Eva Partoll, Fernando Velarde, et al.

BAMS Article

The SALTENA Experiment

Comprehensive Observations of Aerosol Sources, Formation, and Processes in the South American Andes

Federico Bianchi, Victoria A. Sinclair, Diego Aliaga, Qiaozhi Zha, Wiebke Scholz, Cheng Wu, Liine Heikkinen, Rob Modini, Eva Partoll, Fernando Velarde, Isabel Moreno, Yvette Gramlich, Wei Huang, Alkuin Maximilian Koenig, Markus Leiminger, Joonas Enroth, Otso Peräkylä, Angela Marinoni, Chen Xuemeng, Luis Blacutt, Ricardo Forno, Rene Gutierrez, Patrick Ginot, Gaëlle Uzu, Maria Cristina Facchini, Stefania Gilardoni, Martin Gysel-Beer, Runlong Cai, Tuukka Petäjä, Matteo Rinaldi, Harald Saathoff, Karine Sellegri, Douglas Worsnop, Paulo Artaxo, Armin Hansel, Markku Kulmala, Alfred Wiedensohler, Paolo Laj, Radovan Krejci, Samara Carbone, Marcos Andrade, and Claudia Mohr

ABSTRACT: This paper presents an introduction to the Southern Hemisphere High Altitude Experiment on Particle Nucleation and Growth (SALTENA). This field campaign took place between December 2017 and June 2018 (wet to dry season) at Chacaltaya (CHC), a GAW (Global Atmosphere Watch) station located at 5,240 m MSL in the Bolivian Andes. Concurrent measurements were conducted at two additional sites in El Alto (4,000 m MSL) and La Paz (3,600 m MSL). The overall goal of the campaign was to identify the sources, understand the formation mechanisms and transport, and characterize the properties of aerosol at these stations. State-of-the-art instruments were brought to the station complementing the ongoing permanent GAW measurements, to allow a comprehensive description of the chemical species of anthropogenic and biogenic origin impacting the station and contributing to new particle formation. In this overview we first provide an assessment of the complex meteorology, airmass origin, and boundary layer–free troposphere interactions during the campaign using a 6-month high-resolution Weather Research and Forecasting (WRF) simulation coupled with Flexible Particle dispersion model (FLEXPART). We then show some of the research highlights from the campaign, including (i) chemical transformation processes of anthropogenic pollution while the air masses are transported to the CHC station from the metropolitan area of La Paz–El Alto, (ii) volcanic emissions as an important source of atmospheric sulfur compounds in the region, (iii) the characterization of the compounds involved in new particle formation, and (iv) the identification of long-range-transported compounds from the Pacific or the Amazon basin. We conclude the article with a presentation of future research foci. The SALTENA dataset highlights the importance of comprehensive observations in strategic high-altitude locations, especially the undersampled Southern Hemisphere.

KEYWORDS: Aerosol nucleation; Aerosols/particulates; Atmospheric composition; Biosphere/atmosphere interactions; Gas-to-particle conversion; Measurements

https://doi.org/10.1175/BAMS-D-20-0187.1

Corresponding authors: Federico Bianchi, federico.bianchi@helsinki.fi; Claudia Mohr, claudia.mohr@aces.su.se

In final form 17 July 2021

AFFILIATIONS: Bianchi, Sinclair, Aliaga, Zha, Heikkinen, Huang, Enroth, Peräkylä, Xuemeng, Cai, and Petäjä—Institute for Atmospheric and Earth System Research, and Department of Physics, University of Helsinki, Helsinki, Finland; **Scholz and Leiminger**—Institute for Ion and Applied Physics, University of Innsbruck, and Ionicon Analytik Ges.m.b.H., Innsbruck, Austria; **Wu, Gramlich, Krejci, and Mohr**—Department of Environmental Science, Stockholm University, Stockholm, Sweden; **Modini and Gysel-Beer**—Laboratory of Atmospheric Chemistry, Paul Scherrer Institute, Villigen PSI, Switzerland; **Partoll and Hansel**—Institute for Ion and Applied Physics, University of Innsbruck, Innsbruck, Austria; **Velarde, Moreno, Koenig, Blacutt, Forno, and Gutierrez**—Laboratory for Atmospheric Physics, Institute for Physics Research, Universidad Mayor de San Andrés, La Paz, Bolivia; **Marinoni, Facchini, and Rinaldi**—Institute of Atmospheric Sciences and Climate, Italian National Research Council, Bologna, Italy; **Ginot and Uzu**—University of Grenoble Alpes, CNRS, IRD, Grenoble-INP, IGE (UMR 5001), Grenoble, France; **Gilardoni**—Institute of Atmospheric Sciences and Climate, and Institute of Polar Sciences, Italian National Research Council, Bologna, Italy; **Saathoff**—Institute of Meteorology and Climate Research, Karlsruhe Institute of Technology, Karlsruhe, Germany; **Sellegri**—Université Clermont Auvergne, CNRS, Laboratoire de Météorologie Physique, Clermont-Ferrand, France; **Worsnop**—Institute for Atmospheric and Earth System Research, and Department of Physics, University of Helsinki, Helsinki, Finland, and Aerodyne Research, Inc., Billerica, Massachusetts; **Artaxo**—Institute of Physics, University of São Paulo, São Paulo, Brazil; **Kulmala**—Institute for Atmospheric and Earth System Research, and Department of Physics, University of Helsinki, Helsinki, Finland, Aerosol and Haze Laboratory, Beijing Advanced Innovation Center for Soft Matter Science and Engineering, Beijing University of Chemical Technology, Beijing, and Joint International Research Laboratory of Atmospheric and Earth System Sciences, Nanjing University, Nanjing, China; **Wiedensohler**—Experimental Aerosol and Cloud Microphysics, Leibniz Institute for Tropospheric Research, Leipzig, Germany; **Laj**—Institute for Atmospheric and Earth System Research, and Department of Physics, University of Helsinki, Helsinki, Finland, and University of Grenoble Alpes, CNRS, IRD, Grenoble-INP, IGE (UMR 5001), Grenoble, France; **Carbone**—Federal University of Uberlândia, Uberlândia, Brazil; **Andrade**—Laboratory for Atmospheric Physics, Institute for Physics Research, Universidad Mayor de San Andrés, La Paz, Bolivia, and Department of Atmospheric and Oceanic Sciences, University of Maryland, College Park, College Park, Maryland

Here we introduce the Southern Hemisphere High Altitude Experiment on Particle Nucleation and Growth (SALTENA), an international field campaign that took place from December 2017 to May 2018 at the Global Atmosphere Watch (GAW) station Chacaltaya in the Bolivian Andes at 5,240 m MSL. The overall goal of the campaign was to understand the sources, formation and growth mechanisms, and properties of aerosols at this high-altitude research station. The 6-month period was chosen in order to capture the (parts of the) wet (until ~March), transition (~April), and dry season (~May and onward) and the peak season for new-particle-formation events (May; Rose et al. 2015).

Aerosol particles play a fundamental role in Earth's climate system (IPCC 2013; Boucher et al. 2013). Depending on their chemical or physical properties, aerosol particles can influence the climate by interacting directly with solar radiation, or indirectly by acting as cloud seeds [cloud condensation nuclei (CCN) or ice nucleating particles (INP)]. Quantifying aerosol and CCN/INP sources and mechanisms influencing their formation is therefore vital for our understanding of the current and prediction of the future climate. Aerosol particles can either be directly emitted by human or natural activities or be formed in the atmosphere via gas-to-particle conversion processes such as new particle formation (NPF). It is estimated that a significant fraction of CCN (>50%) in the atmosphere arises from NPF (Dunne et al. 2016; Merikanto et al. 2009; Gordon et al. 2016; Kerminen et al. 2018).

An improved understanding of aerosol and CCN/INP sources and formation mechanisms can be achieved by performing in-depth atmospheric observations of precursor gases and aerosols across multiple geographic and climate zones (Kulmala 2018). In situ observations are key to provide information on aerosol and aerosol precursors sufficiently detailed for process

understanding. However, despite the increasing number of such observations, vast areas of the globe such as Africa, South America, and in general the Southern Hemisphere, are poorly characterized (Reddington et al. 2017; Laj et al. 2020). Similarly, observations at high altitudes are scarce, as they involve complex logistics such as aircraft measurements or access to mountain areas. In addition, data interpretation of high-altitude measurements is challenging as it involves understanding of complex interactions between planetary boundary layer, free troposphere, and local orography-driven flows (Coen et al. 2018). Aerosols and their precursor gases are predominantly emitted within the planetary boundary layer (PBL). During their lifetime in the atmosphere, they can undergo several cycles of chemical reactions and phase transition that modify their physical, optical, and chemical properties, and their ability to act as CCN/INP. Aerosols have lifetimes of days to weeks, and once they reach the free troposphere they can be transported across large distances. Observations of aerosol physico-chemical properties at high altitudes, and in places characterized with intense solar radiation, are therefore crucial to improve our understanding of transport and atmospheric removal mechanisms of particles but remain limited to a few sites in Europe and the United States (Bukowiecki et al. 2016; Andrews et al. 2011; Cristofanelli et al. 2013; Bonasoni et al. 2010), Asia (Kivekäs et al. 2009; Osada et al. 2003), and Africa (Gatari et al. 2009; Rodríguez et al. 2009). In addition to CHC, In South America, atmospheric composition observations from high-altitude sites are available from Pico Espejo in Venezuela (Schmeissner et al. 2011; Hamburger et al. 2013) and Cerro Tololo in Chile (Fiebig-Wittmaack et al. 2006).

Located at 5,240 m MSL in the Southern Hemisphere and surrounded by a large variety of complex natural and anthropogenically influenced environments, the Chacaltaya GAW station is the perfect site for such advanced measurements. As shown in the schematic in Fig. 1, this unique observation site in Bolivia is influenced by very different air masses, from the lowlands and the Amazon basin loaded with biogenic emissions (Artaxo et al. 2013; Chauvigné et al. 2019) the Altiplano perturbed by volcanic activity, anthropogenic activities, and Lake Titicaca with its possible organic aerosol precursors emissions (Deng et al. 2021); marine air masses from the Pacific Ocean; anthropogenically influenced air masses from

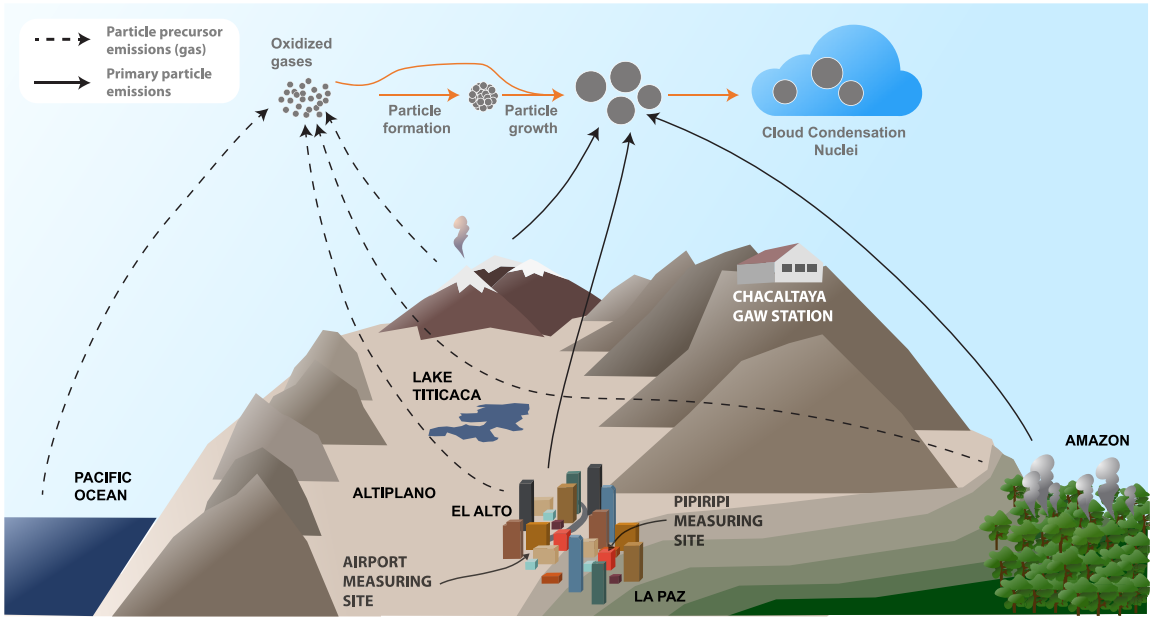

Fig. 1. Schematic of the measurement site and its surroundings. The three measurement stations include Chacaltaya, El Alto, and central La Paz (Pipiripi). The air masses are influenced by the Amazon, the Altiplano and the volcanic activity, and the Pacific Ocean, and by the human activity mainly in La Paz and El Alto.

La Paz–El Alto (Wiedensohler et al. 2018); and air masses containing local and long-range volcanic and biomass-burning emissions.

NPF events are detected regularly at Chacaltaya, with a very high annual frequency (>60% of days) (Rose et al. 2015). While the NPF occurrence has been analyzed at Chacaltaya in detail previously, the chemical description of the events, i.e., the composition of the molecular clusters nucleating to form new particles, and of the compounds contributing to particle growth, has remained lacking. To achieve a complete understanding of particle formation and growth mechanisms, such chemistry-oriented NPF research is fundamental. The technical advancements with respect to state-of-the-art mass spectrometric techniques have only recently made it possible to investigate the chemistry behind NPF, also at remote locations and under the low-pressure conditions of high altitudes (Bianchi et al. 2016, 2021).

Here we present an introduction to the SALTENA campaign. We give a short overview on the history of the Chacaltaya station and describe the overall measurement setup of the field campaign. We also present a brief summary of the analysis of the complex meteorology, airmass origin, and boundary layer–free troposphere interactions using 6-month high-resolution Weather Research and Forecasting (WRF) simulations coupled with Flexible Particle dispersion model (FLEXPART). We then give an overview on the research highlights currently in the focus of our analysis efforts and end with a few concluding remarks on the importance of the station in a changing climate.

SALTENA study design

Overview of the measurement sites. The main site in the SALTENA campaign is the Global Atmosphere Watch (GAW) station CHC located at Chacaltaya (5,240 m MSL; 16.35°S, 68.13°W). The station is located on the northwest face of the mountain with direct view to the metropolitan area of La Paz–El Alto to the southwest. The site samples air masses arriving from the Amazon to the east, the Altiplano (a large high-altitude plateau between 3,800 and 4,100 m MSL) to the west, the Pacific Ocean farther west, and from the La Paz–El Alto metropolitan region (1.7 million inhabitants) located 17 km to the south but 1.1 km below CHC. In addition, given the clear influence of the urban conglomerate on the station, two additional sites were selected for concurrent measurements, one in central La Paz and another at the international airport of El Alto. The former is located on the roof of a Municipal Museum (Pipiripi) at the center of the city of La Paz (3,600 m MSL; 16°30′04′S, 68°07′33″W). This site lies within the perimeter of the central park of La Paz (Parque Urbano Central) and is surrounded by a number of major, heavily trafficked roads (~100 m away). The El Alto site is located within the international airport (4,025 m MSL; 16°30′36.07″S, 68°11′55.48″W) of La Paz–El Alto, and is considerably farther away from any road (minimum distance of 600 m to the nearest street) than the central La Paz site. No influence from airplanes taking off or landing was detected in the past or during the SALTENA campaign, possibly because the runway is far from the station (at least 300 m) to have a noticeable effect on the measurements. The central La Paz station is more representative of curbside conditions, whereas the El Alto station is considered an urban background site. The sites in La Paz and El Alto in addition to CHC were chosen because they allow for investigation of aerosol properties at different altitudes (3,600, 4,025, and 5,240 m MSL) and along the gradient polluted-remote. Together the stations help understand development of the boundary layer and transport of urban pollution to CHC, and aerosol transformation processes during transport.

Campaign instrumentation. For the period of the SALTENA campaign, an extensive set of instruments were added to the permanent measurements provided by the GAW station, in order to allow for measurements of the key species to achieve the experiment objectives and detailed trace gas and aerosol physico-chemical characterization. All instruments (and their abbreviations) used at the three different locations are listed in Table 1. In Table 1 the "data

Table 1. Instrumentation and measured parameters in Chacaltaya, El Alto, and La Paz sites.

Observation type	Instrument name	Measured parameters	Deployment period	Data capture rate during SALTENA
		Chacaltaya (5,240 m MSL)		
Particle physical properties	Particle Size Magnifier (PSM)	Particle number size distribution (1–4 nm)	Dec–May	88%
	Neutral cluster and Air Ion Spectrometer (NAIS)	Particle number size distribution (2–40 nm), ion size distribution (0.8–40 nm)	Permanent	80%
	Mobility particle size spectrometers (MPSS)	Particle number size distribution (10–500 nm)	Permanent	87%
	Condensation Particle Counter (CPC)	Particle number concentration	Permanent	75%
	Single Particle Soot Photometer (SP2)	Black carbon in individual aerosol particles	Apr–May	80%
	Multi Angle Absorption Photometer (MAAP)	Equivalent black carbon	Permanent	81%
	Nephelometer	Aerosol particle optical scattering coefficient	Permanent	90%
	Aethalometer	Black carbon, particle light absorption coefficient	Permanent	90%
Meteorology	3D anemometer	Horizontal and vertical wind speed and direction	Dec–May	>85%
	Automatic Weather Stations (AWS)	Temperature, RH, shortwave and longwave radiation, wind speed and direction, precipitation	Permanent	>70%
Trace gases	Picarro	CO, CO_2, CH_4 mole fraction	Permanent	>83%
	Ozone monitor	Ozone concentration	Apr–Jun	65%
Chemical composition of molecules, ions, and particles (mass spectrometers)	Atmospheric Pressure interface Time-of-Flight (APi-TOF)	Chemical composition of positive and negative ions	Dec–May	85%
	Chemical ionization Atmospheric Pressure interface Time-of-Flight (CI-APi-TOF)	Chemical composition and concentrations of molecules such as sulfuric acid and highly oxygenated organic molecules, trace gases	Dec–May	50%
	Aerosol Chemical Speciation Monitor (ACSM)	Submicrometer nonrefractory aerosol chemical composition	Mar–May	92%
	FIGAERO-CIMS	Concentrations of oxygenated gas and particulate phase organic and inorganic compounds, trace gases	Apr–May	80%
	Proton Transfer Reaction (PTR3)	Trace gases, concentrations of reactive organic carbon compounds	Apr–May	50%
		El Alto (4,025 m MSL)		
Particle physical properties	NAIS	Particle number size distribution (2–40 nm) and ion size distribution (0.8–40 nm)	Mar–May	80%
	MPSS	Particle number size distribution (10–800 nm)	Jan–May	98%
	Aerodynamic Particle Sizer (APS)	Particle number size distribution (500 nm–20 μm)	Jan–May	88%
	SP2 Extended Range (SP2-XR)	Black carbon in individual aerosol particles	Apr–May	60%
	Nephelometer	Aerosol particle optical scattering coefficient	Jan–Jun	93.3%
	Aethalometer	Black carbon, particle light absorption coefficient	Permanent	84%
Meteorology	AWS	Temperature, relative humidity	Permanent	100%
	Anemometer	Horizontal wind speed and direction	Permanent	100%
Trace gases	CO monitor	CO concentration	Permanent	94%
	Ozone monitor	Ozone concentration	Apr–Jun	70.%
Particle chemical composition	ACSM	Submicrometer nonrefractory aerosol chemical composition	Apr–May	89%
		La Paz (3,600 m MSL)		
Particle physical properties	MPSS	Particle number size distribution (10–800 nm)	Jan–May	98%
	APS	Particle number size distribution (500 nm–20 μm)	Jan–May	98%
	SP2-XR	Black carbon in individual aerosol particles	Apr–May	60%
	Aethalometer	Equivalent black carbon, particle light absorption coefficient	Permanent	90%
Meteorology	Anemometer	Horizontal wind speed and direction	Permanent	98%
	Rain gauge	Precipitation	Permanent	100%

capture rate" is the ratio of the time that the instrument was fully operational to the total amount of time that the instrument was installed at the measurement site. We note that at GAW stations, monitors for particulate matter are not a priority, and therefore instruments measuring particle mass are limited at CHC. However, this information can be retrieved from filter-based samples by coupling nephelometer and SMPS measurements.

Meteorology: Observations and model simulations

Meteorological observations. Chacaltaya and the neighboring areas experience complex meteorological conditions driven by a combination of the mountainous terrain and large-scale weather patterns, which result in pronounced diurnal and seasonal cycles. The observed temperature and precipitation at CHC during the 6-month campaign are shown in Fig. 2. They clearly show the transition from wet to dry season, which was one of the reasons why the period from December to May was chosen for the campaign. The average daily mean temperature was 0.2°C (±1.0°C), the average daily maximum was 3.5°C (±1.8°C) and the average daily minimum was −2.3°C (±1.2°C). The temperatures are relatively similar from December to April, whereas generally cooler conditions and larger differences between day and night are evident in May. The 6-month median (mean) daily precipitation was 0.45 (±3.7) mm, with a clear trend showing the wet and dry seasons (austral summer and winter, respectively). Most days between December and March (the wet season) recorded more than 100 mm of precipitation. Precipitation at CHC is primarily in the form of snow, but rain does also occur. The monthly mean relative humidity (RH) exceeded 77% from December to March. In contrast, during the transition from wet to dry season, precipitation and mean RH decreased to 26 mm and 57%, respectively, in April, and 14 mm and 48%, respectively, in May.

Shortwave radiation (irradiance, not shown) also had a seasonal cycle with the highest values in early dry season (May), and lower values from December to February during the wet season.

Comparing in situ observations from the 6-month SALTENA period to long-term meteorological statistics shows good agreement for RH, temperature, and wind speed and direction (not shown), despite a weak La Niña period from November 2017 to March 2018 (Niña-3.4 indices of −0.86 to −0.73; Rayner et al. 2003).

Satellite images provide snapshot examples of the large-scale weather patterns in the wet (Fig. 3a) and dry (Fig. 3b) seasons, corresponding to the start and end of the SALTENA campaign. During the wet season, the intertropical convergence zone (ITCZ) is located south of the equator and convection is extensive across Bolivia, northern Brazil, Peru, and Ecuador. The South Atlantic convergence zone (Carvalho et al. 2004) is

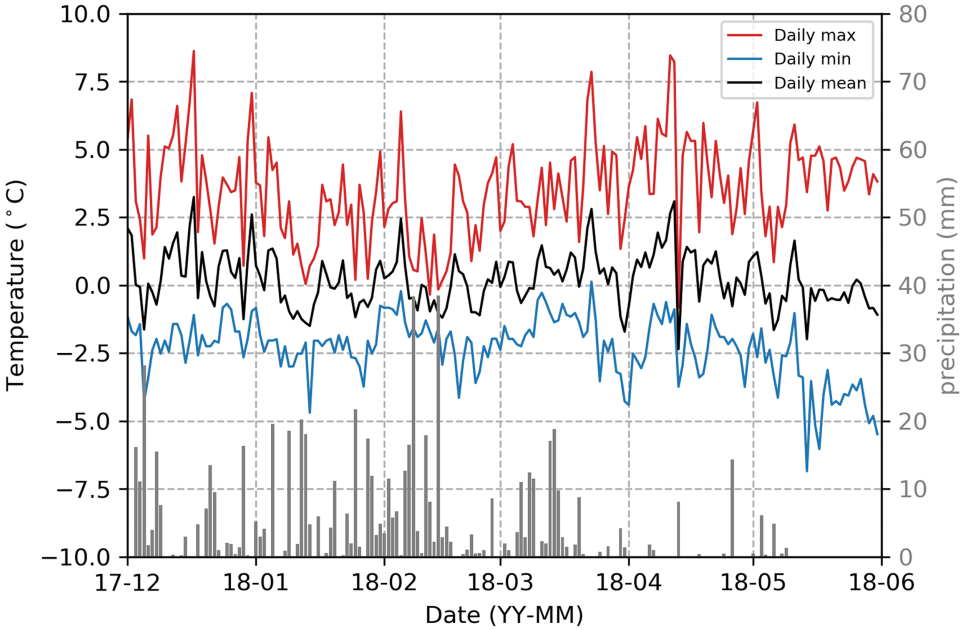

Fig. 2. Time series of the observed daily maximum (red), daily minimum (blue), and daily mean (black) 2-m air temperature measured at CHC at 5,160 m MSL (the main station is located at 5,240 m MSL) from 1 Dec 2017 to 31 May 2018. Gray bars show the daily accumulated precipitation.

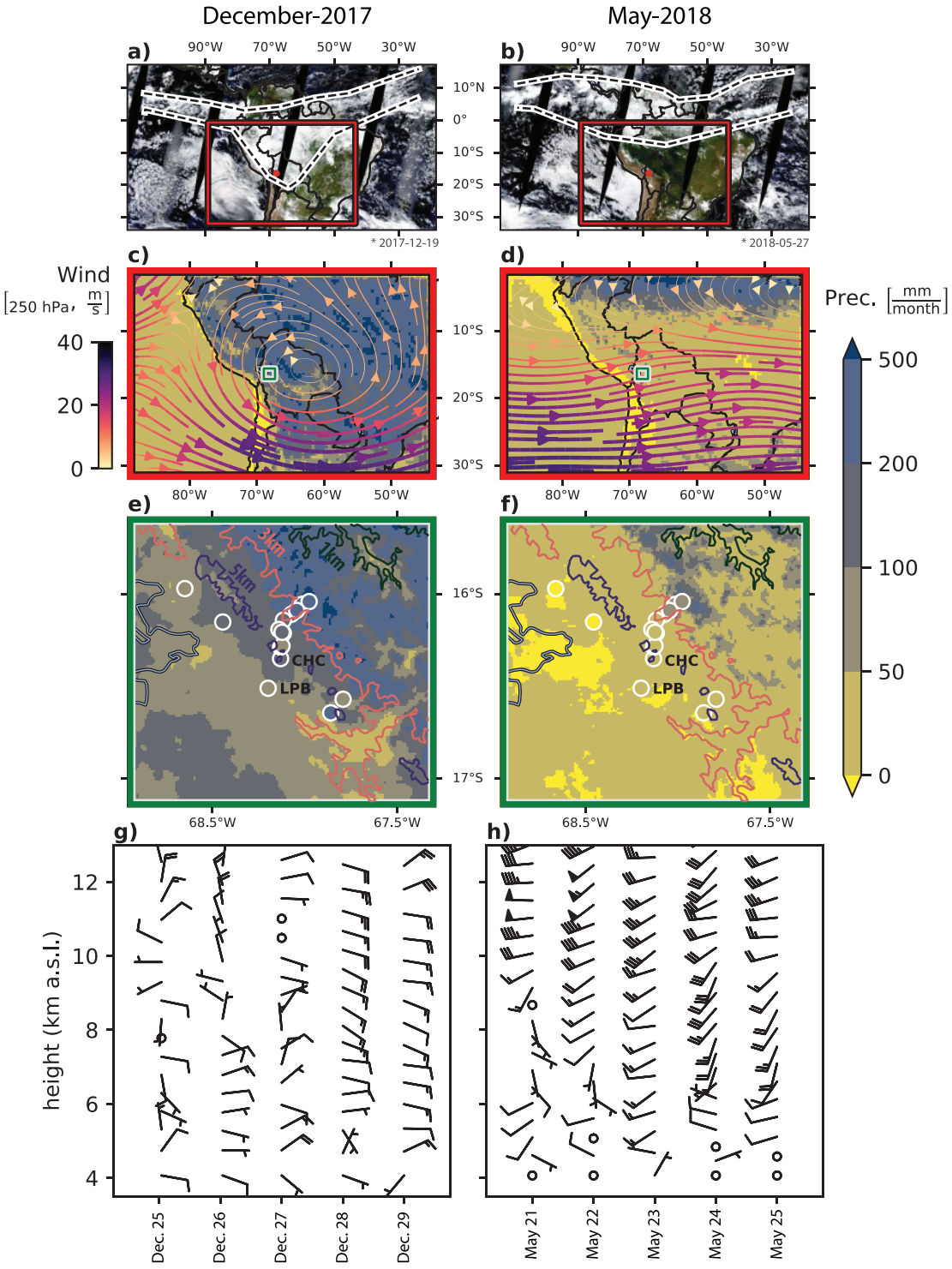

Fig. 3. Meteorological overview. (a),(b) Snapshot satellite images during the SALTENA campaign from NASA Worldview (MODIS_Terra_SurfaceReflectance_Bands143) that are representative of the (a) wet and (b) dry seasons. The dashed lines indicate the approximate location of the intertropical convergence zone (ITCZ). (c),(d) The monthly mean 250-hPa winds (shaded streamlines) and monthly accumulated precipitation (blue shading) from the WRF simulations for (c) December 2017 and (d) May 2018. (e),(f) The zoomed-in monthly accumulated precipitation from WRF near CHC. Colors in the white circles show observations of monthly accumulated precipitation. The purple, orange, and green lines mark the topographic contours at 5, 3, and 1 km MSL, respectively. (g),(h) Wind observations from daily radiosondes released from El Alto at 1200 UTC for 5-day periods that are representative of the (g) wet and (h) dry season. A half barb is 5 kt (~2.5 m s^{-1}), a full barb 10 kt (~5 m s^{-1}), a filled flag 50 kt (~25 m s^{-1}), and an unfilled circle indicates calm conditions. For clarity only every 50th wind observation is plotted. The red box in (a) and (b) shows the largest WRF domain and the green box in (c) and (d) shows the smallest WRF domain.

also evident in the southeast corner of Fig. 3a. During the dry season, the ITCZ is located in a more northerly position meaning that subsidence associated with the descending branch of the Hadley cell (not shown) is present near CHC and thus clear skies prevail over Bolivia.

Radiosondes are launched at 1200 UTC (0800 local time) every weekday from El Alto. These give valuable information about how the temperature, dewpoint and wind speed and direction vary with height and how these vertical profiles vary between the wet and dry seasons. Two representative 5-day periods are shown for December 2017 (Fig. 3g) and May 2018 (Fig. 3h). In the wet season, winds are weak, quite variable between days, and are dominated by easterly winds at most levels. In the dry season, the winds are mainly from the west and are much stronger at upper levels. In both the dry and wet seasons, there are significant changes in the observed wind direction between the surface and 1.5 km AGL, indicating that identifying the origins of air masses is challenging.

Weather Research and Forecasting Model simulations. To complement the meteorological observations and gain additional insight into the dynamics of local and large-scale meteorology, we created a high-resolution gridded meteorological dataset by performing a 6-month simulation with the WRF Model (Skamarock and Klemp 2008) for the SALTENA campaign measurement period. The simulation consisted of four nested domains, the outermost of which had a grid spacing of 27 km and covered a large part of the South American continent (red box in Figs. 3a,b). The innermost domain was centered on CHC, with a grid spacing of 1 km, and covered an area of 154 km × 151 km (green box in Figs. 3e,d). This model configuration enabled us to accurately simulate the small-scale up-valley and up-slope thermally driven winds that control dispersion of air pollution from La Paz–El Alto to CHC and the synoptic-scale weather patterns that influence long-range transport to CHC.

The WRF simulation was verified by comparing observations, primarily from CHC, to the modeled output on hourly, daily, and monthly scales. Reasonable agreement was found, for example, the Pearson's correlation coefficient between the hourly observed and model temperature at CHC was 0.60.

The evolution of the large-scale weather patterns between the wet and dry seasons is also captured well by the WRF simulation (this was ascertained by comparing the WRF monthly mean values of the 500-hPa height, the 250-hPa wind speed, and precipitation) to those from reanalysis datasets (not shown). The monthly mean 250-hPa (approximately 11 km MSL) winds from our WRF simulation are shown for December 2017 (Fig. 3c) and May 2018 (Fig. 3d). In December, an upper-level anticyclone—the Bolivian high (Lenters and Cook 1997)—is present, which results in easterly winds at upper levels. In contrast, the upper-level mean circulation in May 2018 shows the zonally oriented subtropical jet on the southern edge of the WRF domain (Fig. 3d). The observed and WRF-simulated monthly accumulated precipitation values are also shown for December 2017 (Fig. 3e) and May 2018 (Fig. 3f). On monthly scales, reasonable agreement is found between the model precipitation and observed precipitation. In December 2017, the simulated monthly accumulated precipitation at CHC was 124 and 81 mm in El Alto and the corresponding observed values were 146 and 75 mm, respectively. These relatively high values are due to the prevailing easterly to northeasterly winds at the surface (Fig. 3g) that transport moisture from the Amazon to CHC, which combined with high levels of incoming solar radiation (especially when only scattered clouds are present) and the lack of any large-scale subsidence, drives deep convection typically during daytime (as evident in Fig. 3a). At nighttime, however, precipitation is mainly stratiform in structure

(Perry et al. 2017) but still fueled by the influx of Amazonian moisture. In May 2018, the precipitation accumulations were much lower; 1 mm of precipitation was simulated at CHC and 0 mm at El Alto. The observed values were 14 and 11 mm. These very low precipitation amounts occur due to large-scale subsidence at the edge of the Hadley cell and limited moisture sources: the moist air masses of the Amazon are not transported to CHC during May and neither are the moist air masses that are present over the South Pacific, as a stable inversion and the steep barrier of the Andes prevents transport to CHC (Falvey and Garreaud 2005).

Airmass origin. To fully understand the changes in atmospheric composition during SALTENA, the measurements of trace gas and aerosol properties must be combined with detailed information about the local meteorology and airmass origin. Therefore, in addition to using local meteorological observations and the WRF simulation, output from the high-resolution WRF simulations was used to drive backward trajectories with the Lagrangian dispersion model FLEXPART (Brioude et al. 2013). The FLEXPART simulations, which cover the same domain as the WRF simulations and have similar spatial resolution, allowed us to identify source regions of air masses arriving at CHC and determine whether the station was influenced by boundary layer, residual layer, or free-tropospheric air masses. This source area identification method and the WRF and FLEXPART simulations are discussed in detail by Aliaga et al. (2021).

Research highlights

Unraveling chemical transformation processes of anthropogenic pollution during transport from the boundary layer to the free troposphere. The comprehensive instrumentation deployed across three measurement sites during the SALTENA campaign permitted an unprecedented look at the changes in the physico-chemical properties of polluted air as it is transported from anthropogenic source regions in the Altiplano, including the metropolitan areas of La Paz–El Alto, to the high-altitude station CHC and the free troposphere. The observations will enable further investigation of (i) specific urban sources of pollution in the undersampled Southern Hemisphere; (ii) anthropogenic aerosol ageing processes including secondary formation under strong solar radiation conditions due the high altitude; (iii) the role of atmospheric pollutants in NPF and growth of particles to sizes relevant for cloud formation; and (iv) the potential climatic and environmental impacts of the pollution across the broader Altiplano and Andes region of the South American continent.

Figures 4a and 4b show the difference in campaign-average diurnal pattern and relative contribution to submicron particulate matter (PM_1) of particulate compounds measured in El Alto and CHC. The chemical composition of $PM_{2.5}$ (PM with a diameter of up to 2.5 mm) was not measured during SALTENA; currently ongoing analyses of filter-based samples of PM_1 and $PM_{2.5}$ collected during the years prior to SALTENA at CHC will be the focus of a separate study. Concentrations in El Alto peaked at 0700 and 2000 local time corresponding to rush-hour times, and the average submicron chemical composition was dominated by black carbon and organic matter (of both primary and secondary origin). This supports findings from an earlier study of Wiedensohler et al. (2018), who took advantage of a unique, traffic-free situation on the Bolivian Day of Census in 2012 to estimate that traffic-related emissions account for a high 80% of the PM_1 pollution (including black carbon) in the metropolitan area of La Paz–El Alto. One of our SALTENA-based research foci will include detailed analyses of the traffic-related emissions of organic matter, the mass spectra of which indicate a very high contribution of hydrocarbons (not shown), and black carbon properties (see further down) and their implications for air quality and human health in El Alto.

The CHC diurnal pattern with its peak around noon visualizes how the PBL containing pollution from the source regions in the Altiplano such as the metropolitan area of La Paz–El

Alto develops to the altitude of the station during the morning hours. Compared to El Alto, the submicron particle chemical composition was more dominated by secondary inorganic particle components, especially sulfate (which will be discussed later), and a more aged organic aerosol (not shown), as indicated by mass spectral features similar to these reported by Ng et al. (2011). The detailed characterization of (photo-)chemical processing of air masses during transport from the source regions to CHC, and molecular composition of organic aerosol particles at such altitudes are the focus of ongoing analyses. These are greatly helped by the suite of state-of-the-art mass spectrometers deployed at CHC during SALTENA (see Table 1). Figures 4c and 4d show as an example the average diurnal pattern (9–23 May) of organic molecules containing seven carbon atoms and different numbers of oxygen, hydrogen, and nitrogen atoms in the gas and particle phases at CHC. These are likely related to toluene (C_7H_8), one of the most abundant anthropogenic aromatic hydrocarbons (Henze et al. 2008) and its oxidation products (Ji et al. 2017; Molteni et al. 2018). Such detailed molecular-level information will help us not only further specify sources and oxidation reactions of organics emitted within the PBL, but also, e.g., parameterize climate-relevant aerosol properties such as hygroscopicity and volatility (Deng et al. 2018; Mohr et al. 2019).

Black carbon (BC) is of particular interest for the region: it is not only a concern for human health in the La Paz–El Alto urban area, but has likely also played a role in accelerating the retreat of Andean glaciers and snow cover over recent decades by decreasing the surface albedo of ice-covered surfaces through deposition, and thereby speeding up their melting process (de Magalhães et al. 2019; Vuille et al. 2018). To investigate the transport of anthropogenic emissions from La Paz–El Alto to high altitudes, we combined the high-resolution WRF simulations with FLEXPART back trajectory modeling (see "Meteorology" section), BC concentration measurements, and elastic net regression (Pedregosa et al. 2011) to identify the specific source regions of the BC measured in the air at CHC. We note that the La Paz–El Alto region is also a source of other

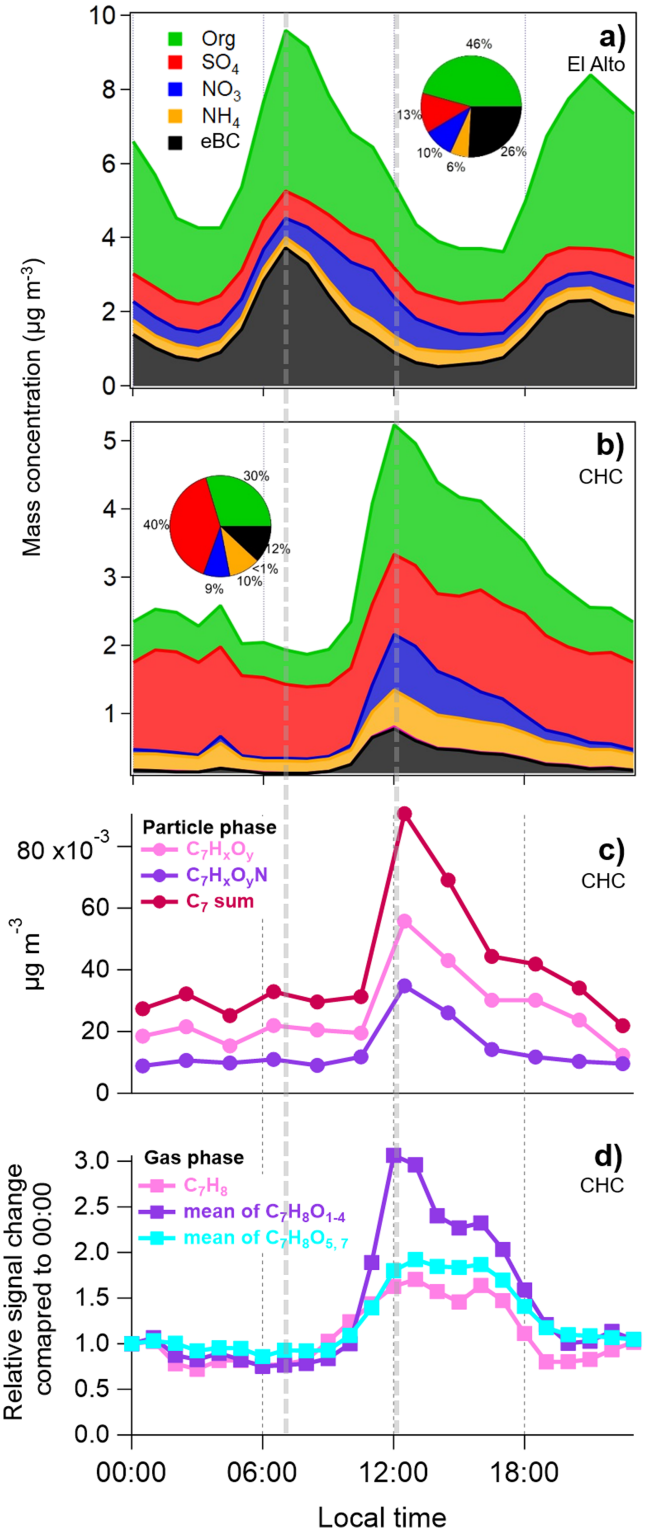

Fig. 4. Diel patterns of Organic matter (Org), sulfate (SO_4), nitrate (NO_3), and ammonia (NH_4) measured by ACSM, and equivalent black carbon (eBC) measured by an aethalometer in (a) El Alto and (b) Chacaltaya (<1% refer to chloride). The diel patterns of C7 compounds in the (c) particle phase and (d) gas phase shown are measured by FIGAERO-CIMS, PTR3, and CI-APi-TOF. The vertical dashed lines guide the eye to show the local time of day when concentrations peak in El Alto and Chacaltaya, respectively. The data shown cover 9–23 May during which the area was governed by typical dry season meteorology.

aerosol components such as nitrate, sulfate, or organic matter, but use here BC due to its unambiguous origin (outside the biomass-burning season) for anthropogenic source region identification. Figure 5a displays the results of the BC footprint analysis, where the probabilities that individual grid cells (P_w) are source regions for the BC measured at CHC are overlaid onto a map of the surrounding area. An extremely clear "hot spot" of emissions probability is located directly over La Paz and El Alto, confirming that this urban area is the dominant source of the high levels of BC aerosol that reach CHC and, presumably, other surrounding mountains.

Measurements of refractory BC (rBC) particle core size distributions at the three measurement sites of the SALTENA campaign (see "SALTENA study design" section) give further insights into the changes of BC with residence time in the atmosphere and transport to CHC (Fig. 5b). The very small BC particle core sizes (<100 nm) at the central La Paz site, which is surrounded by heavily trafficked roads, support the conclusion that traffic is the dominant source of BC in La Paz (e.g., Wiedensohler et al. 2018). At the urban background site of El Alto, which is further from traffic sources than the La Paz site, the median BC core size distribution is shifted to much larger values, with a peak observed around 190 nm. Since the organic aerosol mass spectra recorded by the Aerosol Chemical Speciation Monitor (ACSM) at El Alto did not possess any biomass-burning markers, we rule out biomass burning as a major BC source. We therefore hypothesize that the much larger BC cores at El Alto compared to the La Paz site are the result of rapid ageing (e.g., coagulation) and/or mixing and dilution with larger, aged BC particles as the particles are advected away from the heavily trafficked roads. The shapes of the BC core size distributions measured during boundary layer influenced conditions at CHC are very similar to the El Alto distributions, which strengthens the conclusion from the

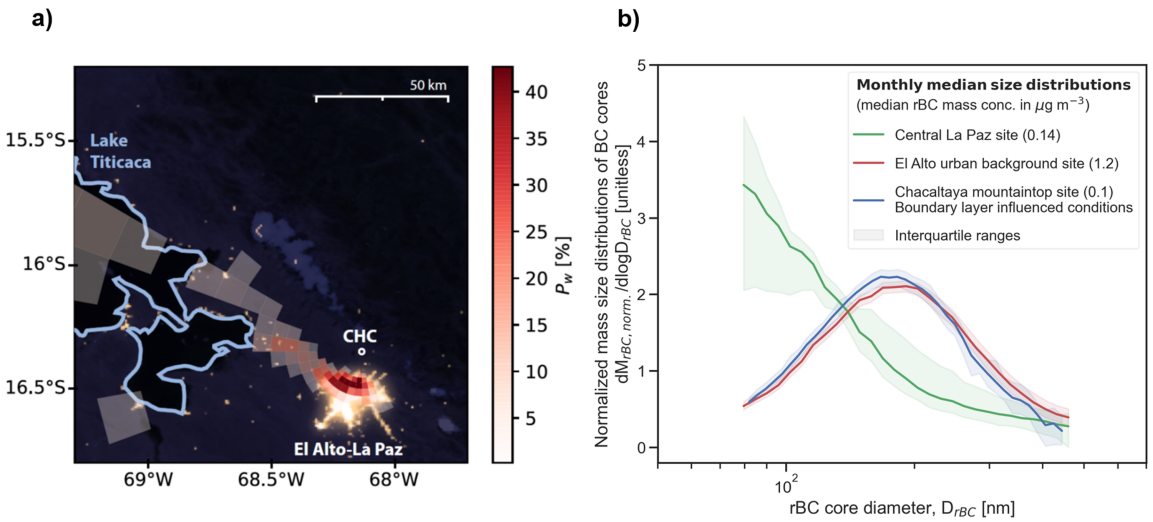

Fig. 5. (a) Potential grid cell sources of BC influencing CHC during the campaign period (December 2017–May 2018), overlaid over a nighttime satellite picture from NASA (https://earthdata.nasa.gov/eosdis/science-system-description/eosdis-components/gibs#ed-gibs-citation) to show the city limits of La Paz–El Alto. Increasing probability weight (P_w) values indicate higher likeliness of the cell to be a source region for BC. Local topography and the closeness to CHC favor the likeness of the northern part of the city. (b) Median mass size distributions of refractory black carbon (rBC) cores measured at the three SALTENA measurement stations (central La Paz, El Alto, and Chacaltaya) for the period from 24 Apr to 19 May. Shaded areas represent the interquartile ranges of each of the median mass size distributions. The Chacaltaya results only include mass size distributions measured during boundary layer influenced conditions, which are defined as occurring between 1000 and 1400 LT. The mass size distributions have been normalized by dividing by the median integrated rBC mass concentration measured at each site, which are displayed in parentheses in the figure legend.

footprint analysis (Fig. 5a) that La Paz–El Alto is a major source region of the BC measured at CHC. Further investigation of the BC transport and ageing processes during SALTENA is currently being undertaken and will be discussed in the context of potential regional climate effects in a separate publication.

Volcanic activities in the Altiplano as a source of atmospheric sulfur components. The SALTENA campaign has revealed the Altiplano to be a significant source of atmospheric sulfur-containing compounds in the gas and particle phase due to the volcanic activity in the region. Especially the Sabancaya volcano in Peru was active during the measurement campaign, and CHC was impacted by its plume as shown by the December 2017–May 2018 SO_2 column amount derived from satellite images (filtered for outliers; Li et al. 2020) in Fig. 6a. Figure 6b shows the time series of particulate sulfate concentrations, which exhibited particularly high loadings during May when the station was impacted by Altiplano air masses (Aliaga et al. 2021). Volcanic emissions do not only directly affect particulate sulfate concentrations, but aerosol chemistry in many ways, as exemplified in Fig. 6c. Here we compare the sulfur-containing compounds in the gas and particle phases for the periods when volcano plumes were encountered (7–9 and 21–23 May 2018), and the periods less impacted by volcanic emissions (11–13 and 29–31 May 2018). During the volcanic episodes, a higher fraction of sulfur-containing ions ($H_xS_yO_z^-$, sulfuric acid and its clusters are not included) in the gas phase and a higher mass fraction of sulfur-containing compounds including organosulfates (CHOS) and nitroxy organosulfates (CHONS) in the particle phase were observed. SO_2 emitted from volcanic activities and its oxidation products may also play a role in atmospheric NPF observed regularly at CHC, especially during the dry season.

The chemical components involved in new particle formation. With the mass spectrometers deployed during SALTENA (see Table 1) we have the unprecedented opportunity to elucidate the chemical components involved in NPF observed regularly at CHC, and to unravel the contributions of compounds from the (polluted) PBL and the free troposphere. An instructive way

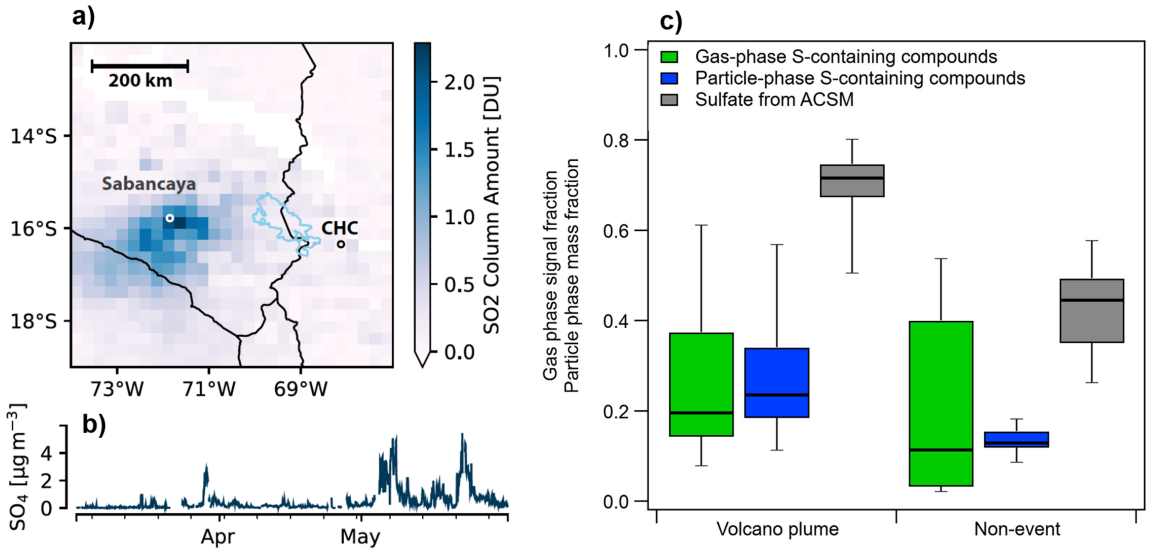

Fig. 6. (a) Average SO_2 concentration in the atmospheric column from December 2017 to May 2018 derived from the ozone monitoring instrument (OMI) on board the *Aura* satellite; (b) time series of particulate sulfate measured by ACSM in Chacaltaya; and (c) box-and-whisker plots of signal fraction of S-containing compounds (SO_3^-, SO_4^-, SO_5^-, HSO_3^-, etc., except H_2SO_4) in the gas phase measured by the APi-TOF (green) and mass fraction of S-containing organic compounds in the particle phase measured by the FIGAERO-CIMS (blue), as well as particulate sulfate by the ACSM (gray) during volcano plumes and non-volcano plume days in Chacaltaya.

to present a mass spectrum is the mass defect plot, where the abscissa represents the measured mass (mass-to-charge ratio m/z, with $z = 1$ in atomic mass units, amu) of the compounds and the ordinate their mass defect, which is the difference between the accurate mass and the nominal mass (Bianchi et al. 2014). In Fig. 7 we show a mass defect plot of negative naturally charged ions nucleating during a NPF event in April 2018. The symbol size is proportional to the peak intensity. Sulfuric acid clusters of various sizes and composition make up the largest fraction of the signal (red and orange clusters). Sulfuric acid–ammonia clusters reaching a mass of 1,200 amu and above were observed in previous laboratory experiments (Bianchi et al. 2014), and these large clusters are also probably one of the important drivers of NPF. A cluster with a size of 1,200 amu corresponds to an estimated mobility equivalent diameter of 1.8 nm (Mäkelä et al. 1996; Steiner et al. 2014). Signals of organic compounds were not negligible, especially in the mass range of 200–600 amu. The role of organic compounds in NPF at CHC is currently under investigation. Simultaneous measurements of cluster and particle number size distributions at CHC and El Alto (Fig. 8) show NPF to happen at both locations. The measurements are thus very useful to understand the regional extent of this phenomenon, as well as the role that emissions from the boundary layer, convective uplifting, and transport of air masses from the free troposphere play for nucleation and growth of particles at CHC/this region.

Free-tropospheric air masses and what they contain. The high altitude of the station also allowed for glimpses into the chemical composition of compounds in the free troposphere, and to assess long-range transport of compounds from such diverse sources as the lowlands to the east of the Cordillera Real where the station is located, the Amazon region, and the Atlantic Ocean, or, to the west, the Pacific Ocean. An earlier study investigating the role of topography for the PBL influence on mountain stations (Coen et al. 2018) ranked CHC roughly in the middle when comparing the PBL influence for all mountain stations around the globe. Also, Rose et al. (2017) concluded that only during the night a significant fraction of the air impacting the station would be from the free troposphere.

In addition to the detailed grid cell source analysis by Aliaga et al. (2021) (see "Meteorology" section), we also used the water vapor mixing ratio measured at CHC as an indicator for free-tropospheric air, especially for intrusions not captured by the previously mentioned modeling work. The average water vapor mixing ratios under non-free-tropospheric conditions in the wet and dry seasons were 6.0 ± 0.6 g kg^{-1} and 3.4 ± 1.6 g kg^{-1}, respectively. In contrast, the water mixing ratios determined in the free-troposphere air were lower (5.0 ± 0.5 g kg^{-1} and 1.1 ± 0.3 g kg^{-1} for the wet and dry seasons, respectively).

We hypothesized earlier that free-tropospheric air masses should contain compounds representative

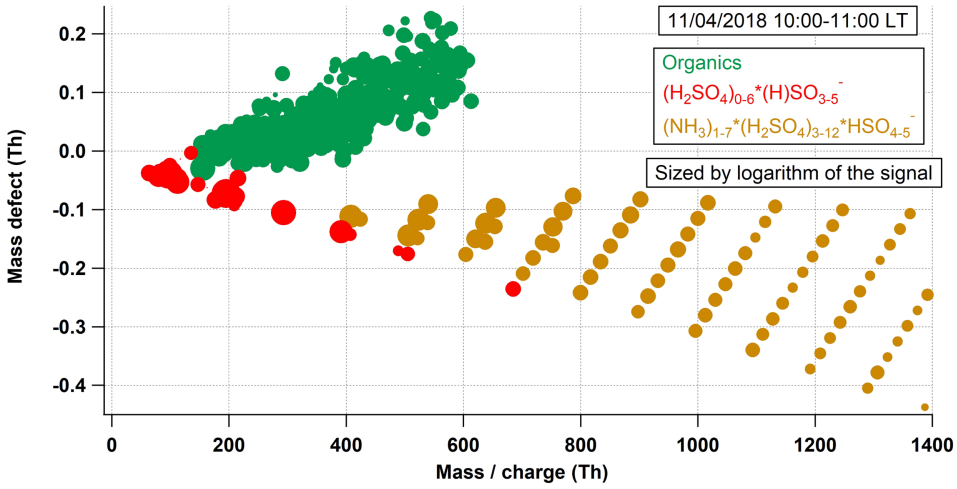

Fig. 7. Mass defect plot of the negative naturally charged ions in counts per second (cps) measured by the APi-TOF during an NPF event observed on 11 Apr 2018. Each dot represents a cluster with a unique ionic composition (green: organic ions; red: clusters of pure sulfuric acid; orange: clusters composed solely by sulfuric acid and ammonia). The largest clusters detected contain up to 13 molecules of sulfuric acid and 7 molecules of ammonia.

of source regions far away from CHC, such as the Amazon or the Pacific Ocean. Examples would be oxidation products of biogenic organic compounds (Amazon) such as highly oxygenated organic molecules (HOM) and of dimethyl sulfide emitted by marine phytoplankton such as methane sulfonic acid (MSA). Figures 9a and 9c show the frequency distributions of the concentrations of HOM for January (wet season, large-scale easterly winds) and MSA for May (dry season, large-scale westerly winds). The respective time series are shown in Figs. 9b and 9d. Bars colored in orange denote concentration values for periods

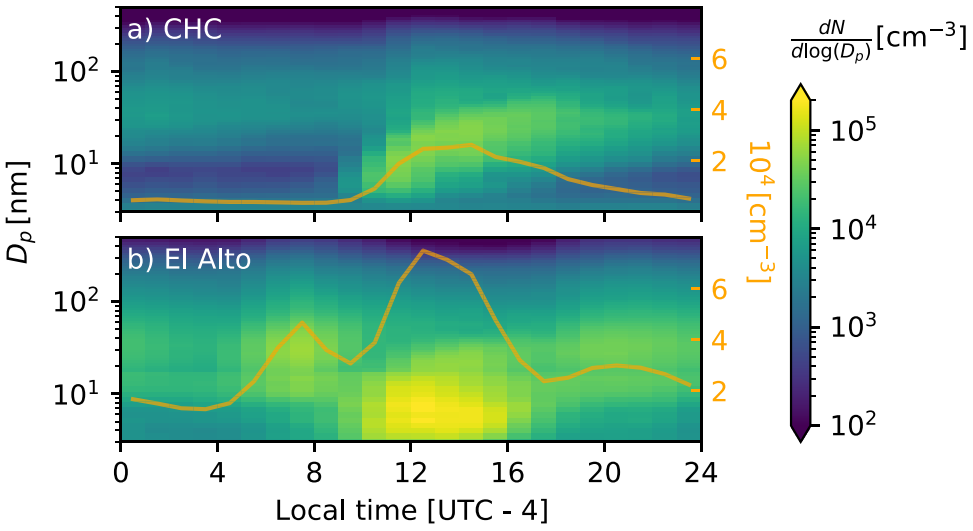

Fig. 8. May 2018 diurnal median particle size distributions sampled at (a) CHC and (b) El Alto. The 3–18-nm range is shown using observations from the Neutral cluster and Air Ion Spectrometer (NAIS) in negative neutral particle mode. The 18–500-nm range is shown with observations from the mobility particle sizer spectrometer (MPSS). The orange curve is the integrated particle number concentration from 3 to 500 nm for each location.

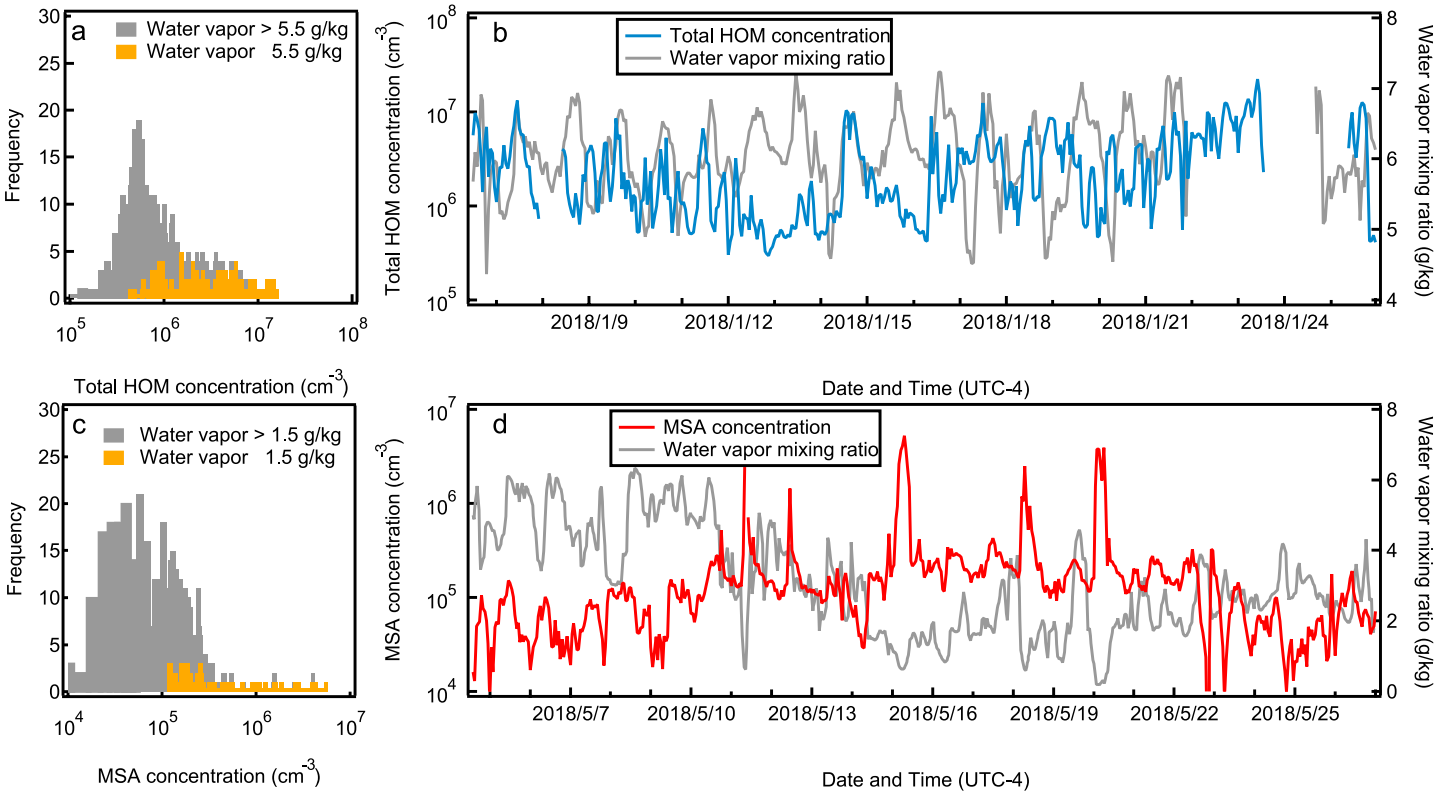

Fig. 9. (a) Frequency distribution and (b) time series of concentrations of highly oxygenated organic molecules (HOM) for January (wet season, in blue) and (c) frequency distribution and (d) time series of the concentrations of methane sulfonic acid (MSA) in May (dry season, in red). The time series of water vapor mixing ratio is also shown for both months (in gray). The gray and orange bars in (a) and (c) denote concentration values for periods when the water vapor mixing ratio was above and below a certain threshold (5.5 g kg^{-1} for the wet season and 1.5 g kg^{-1} for the dry season).

History of the Chacaltaya GAW station

Scientific observations at Mount Chacaltaya have a long history (Fig. SB1). Although the site is well-known for discoveries concerning cosmic rays, the first observations were related to meteorological measurements, when in 1942 a weather station was set up by Bolivian scientist Ismael Escobar near where the current infrastructure is located today. The interest in observations of cosmic rays at high-altitude sites at that time motivated the search for adequate locations. Chacaltaya was (and still is) an excellent site, not only due to its altitude, but also to its location in the Southern Hemisphere, which faces the center of our galaxy. In 1947, Brazilian physicist Cesar Lattes, who at that time was part of an English group led by Cecil Powell at the University of Bristol, took nuclear emulsion plates to detect charged particles to Chacaltaya. These plates allowed scientists to detect tracks left behind by those particles when they passed through.

The Bristol group's goal was to improve the observations made the previous year by Giuseppe Occhialini at the French Pyrenees mountain of Pic-du-Midi (2,877 m MSL) where they detected a particle never observed previously. To confirm the discovery, Lattes took the plates to Chacaltaya, where a larger number of events that lead to the production of this particle were expected. Soon thereafter, the discovery of π-meson was confirmed and some of its properties were finally established with the data obtained at Chacaltaya. This particle was the elusive pion predicted by Japanese physicist Hideki Yukawa, who received the Nobel Prize in 1949 for his work. One year later, in the 1950s, Cecil Powel was also awarded the Nobel Prize for the experimental confirmation of the existence of Yukawa's pion.

Fig. SB1. Picture of the Chacaltaya GAW station. The mountain behind the station is Mount Chacaltaya, which is just 100 m above the measurement site. The Cumbre site, where meteorological observations and aerosol filter sampling are carried out, is visible on the ridge behind the station.

In 1952, the Brazilian Center for Research in Physics led by Lattes, joined forces with Bolivia's University Mayor de San Andres (UMSA) to build a cosmic ray laboratory on Mount Chacaltaya. This action would later become an important step for cosmic ray research in Latin America. At the end of that decade, Lattes and Yukawa promoted scientific collaboration between Brazil and Japan, which was carried out successfully at Chacaltaya for almost three decades. The observatory is still active in cosmic rays although a new, large experiment is being set up at a lower part of the mountain; this time led by 2015 Nobel Prize Laureate Takaaki Kajita from Japan.

In the meantime, atmospheric research returned to Chacaltaya led by the UMSA's Laboratory for Atmospheric Physics when a proposal to the Global Atmosphere Watch (GAW) network from the World Meteorological Organization was accepted to establish a regional station there. The CHC station was set up in December 2011 by an international consortium led by UMSA and partners from France, Germany, Sweden, Spain, and the United States, and has been working continuously ever since, except for a 4-month gap between September 2019 and January 2020, required to perform substantial maintenance to the electric grid. Its unique location, also for atmospheric sciences, makes it ideal for studying transport of anthropogenic compounds into the free troposphere, processes such as the impact of large human settlements on the local and regional atmosphere, effects of long-term transport of products from biomass burning on the Andean glaciers and new particle formation under very different environmental conditions.

Observations over the past 10 years have produced a number of new results related to new particle formation (Rose et al. 2015) and its impact on CCN production (Rose et al. 2017), variability of black carbon (Chauvigné et al. 2019) and mercury (Koenig et al. 2021), and the impact of La Paz–El Alto on atmospheric composition at CHC (Wiedensohler et al. 2018). A number of other studies are in preparation.

Today, CHC is one of the few active GAW stations in South America, especially in the Andean mountains, with the capacity to host large-scale experiments, like SALTENA, as part of international collaborations.

when the water vapor mixing ratio was below a certain threshold (5.5 g kg^{-1} for the wet season and 1.5 g kg^{-1} for the dry season), i.e., when the likelihood of tropospheric air impacting the station was high. The highest values of both HOM and MSA concentrations were found during periods with the lowest water vapor mixing ratio; Figs. 9b and 9d show an anticorrelation for the entire period. This suggests that free-tropospheric air carries gaseous species that are oxidation products of a marine compound from the Pacific and biogenic compounds emitted in the lowlands/Amazon region. Our detailed chemical composition measurements at CHC during SALTENA therefore help identify and characterize the compounds that undergo

long-range transport in the atmosphere and therefore influence climate-relevant processes far away from their source regions (here CHC can be regarded both as an impactor site, but also as a source region for aerosols transported, e.g., to the remote Pacific Ocean (Shank et al. 2012; Bourgeois et al. 2015).

Concluding remarks

The first results from the SALTENA observations highlight the importance of continuous comprehensive observations in strategic locations such as the Chacaltaya GAW station. The decade-long history of atmospheric measurements at CHC have laid the ground for this intensive measurement campaign. Thanks to the deployment of the extensive set of instruments during SALTENA it will be possible to characterize the multitude of activities that affect the free troposphere above the tropical Andes. These activities include anthropogenic emissions from polluted cities (La Paz and El Alto), but also natural phenomena such as sporadic volcanic activities from the Altiplano or biogenic emissions from the Amazon forest, which can reach high altitudes and affect aerosols and cloud formation. Our future work will allow for detailed studies on these sources and their impact on Chacaltaya and the Andes in general, such as for example making the connection between biogenic emissions and the large number of particles that have been observed earlier at high altitudes above the Amazon (Andreae et al. 2018).

As in many locations across the globe, meteorology and seasonality play a crucial role for emissions, concentrations, and properties of natural and anthropogenic atmospheric constituents. At Chacaltaya, the prevailing wind is strongly connected to season (wet, easterly winds versus dry, westerly winds); with SALTENA we were able to cover the wet and wet-to-dry transition seasons as well as 1 month of the dry season. Future efforts should therefore focus on a commitment to keeping CHC running despite logistical challenges, and to invest in expanding its observational capabilities. This is of fundamental importance to capture the different features observed in different seasons, catch unpredictable events such volcanic eruptions or long-range transportation from the Pacific Ocean or the Amazon forest.

The SALTENA experiment is motivated by the idea of improving our knowledge on natural and anthropogenic aerosols observed at high-altitude sites and their formation processes. Continuous measurements will also allow us to understand the impact of environmental changes such as land use changes in the Altiplano or Amazon basin and the fast growing urban areas in Latin America on the atmospheric composition and its implications for air quality and climate change.

Acknowledgments. We thank the Bolivian staff of the IIF-UMSA (Institute for Physics Research, UMSA) who work at CHC for their valuable work under difficult conditions and the IRD (Institute for Research and Development) personnel for the logistic and financial support during all the campaign including shipping and customs concerns. We also acknowledge the CSC–IT Center for Science, Finland, for generous computational resources that enabled the WRF and FLEXPART-WRF simulations to be conducted. We thank the European Union (EU) H2020 program via the findings European Research Council (ERC; project CHAPAs 850614 and ATM-GTP 742206) and the Marie Skłodowska Curie (CLOUD-MOTION 764991), the Finnish Centre of Excellence as well as the Academy of Finland (projects 311932, 315203, and 337549), and the Knut and Alice Wallenberg Foundation (WAF project CLOUDFORM 2017.0165). P. Artaxo acknowledge funds from FAPESP (Fundação de Amparo à Pesquisa do Estado de São Paulo) Grant 2017/17047-0.
The long-term observations used in SALTENA are performed within the framework of GAW and ACTRIS, receiving support from UMSA, and from the international stakeholders. In France, support from CNRS through ACTRIS-FR/SNO CLAP, and IR DATA TERRA, Institut de Recherche et Développement (IRD) and Observatoire des Sciences de l'Univers de Grenoble (OSUG) through ANR LABEX in particular is greatly acknowledged.
We acknowledge the use of imagery provided by services from NASA's Global Imagery Browse Services (GIBS), part of NASA's Earth Observing System Data and Information System (EOSDIS).

References

Aliaga, D., and Coauthors, 2021: Identifying source regions of air masses sampled at the tropical high-altitude site of Chacaltaya using WRF-FLEXPART and cluster analysis. *Atmos. Chem, Phys.,* **21**, 16 453–16 477, https://doi.org/10.5194/acp-21-16453-2021.

Andreae, M. O., and Coauthors, 2018: Aerosol characteristics and particle production in the upper troposphere over the Amazon Basin. *Atmos. Chem. Phys.*, **18**, 921–961, https://doi.org/10.5194/acp-18-921-2018.

Andrews, E., and Coauthors, 2011: Climatology of aerosol radiative properties in the free troposphere. *Atmos. Res.*, **102**, 365–393, https://doi.org/10.1016/j.atmosres.2011.08.017.

Artaxo, P., and Coauthors, 2013: Atmospheric aerosols in Amazonia and land use change: From natural biogenic to biomass burning conditions. *Faraday Discuss.*, **165**, 203–235, https://doi.org/10.1039/c3fd00052d.

Bianchi, F., and Coauthors, 2014: Insight into acid-base nucleation experiments by comparison of the chemical composition of positive, negative, and neutral clusters. *Environ. Sci. Technol.*, **48**, 13 675–13 684, https://doi.org/10.1021/es502380b.

——, and Coauthors, 2016: New particle formation in the free troposphere: A question of chemistry and timing. *Science*, **352**, 1109–1112, https://doi.org/10.1126/science.aad5456.

——, and Coauthors, 2021: Biogenic particles formed in the Himalaya as an important source of free tropospheric aerosols. *Nat. Geosci.*, **14**, 4–9, https://doi.org/10.1038/s41561-020-00661-5.

Bonasoni, P., and Coauthors, 2010: Atmospheric brown clouds in the Himalayas: First two years of continuous observations at the Nepal Climate Observatory-Pyramid (5079 m). *Atmos. Chem. Phys.*, **10**, 7515–7531, https://doi.org/10.5194/acp-10-7515-2010.

Boucher, O., and Coauthors, 2013: Clouds and aerosols. *Climate Change 2013: The Physical Science Basis*, T. F. Stocker et al., Eds., Cambridge University Press, 571–658.

Bourgeois, Q., A. M. L. L. Ekman, and R. Krejci, 2015: Aerosol transport over the Andes from the Amazon Basin to the remote Pacific Ocean: A multiyear CALIOP assessment. *J. Geophys. Res. Atmos.*, **120**, 8411–8425, https://doi.org/10.1002/2015JD023254.

Brioude, J., and Coauthors, 2013: The Lagrangian particle dispersion model FLEXPART-WRF version 3.1. *Geosci. Model Dev.*, **6**, 1889–1904, https://doi.org/10.5194/gmd-6-1889-2013.

Bukowiecki, N., and Coauthors, 2016: A review of more than 20 years of aerosol observation at the high altitude research station Jungfraujoch, Switzerland (3580 m asl). *Aerosol Air Qual. Res.*, **16**, 764–788, https://doi.org/10.4209/aaqr.2015.05.0305.

Carvalho, L. M. V., C. Jones, and B. Liebmann, 2004: The South Atlantic convergence zone: Intensity, form, persistence, and relationships with intraseasonal to interannual activity and extreme rainfall. *J. Climate*, **17**, 88–108, https://doi.org/10.1175/1520-0442(2004)017<0088:TSACZI>2.0.CO;2.

Chauvigné, A., and Coauthors, 2019: Biomass burning and urban emission impacts in the Andes Cordillera region based on in situ measurements from the Chacaltaya Observatory, Bolivia (5240 a.s.l.). *Atmos. Chem. Phys.*, **19**, 14 805–14 824, https://doi.org/10.5194/acp-19-14805-2019.

Coen, M. C., and Coauthors, 2018: Identification of topographic features influencing aerosol observations at high altitude stations. *Atmos. Chem. Phys.*, **18**, 12 289–12 313, https://doi.org/10.5194/acp-18-12289-2018.

Cristofanelli, P., and Coauthors, 2013: Influence of biomass burning and anthropogenic emissions on ozone, carbon monoxide and black carbon at the Mt. Cimone GAW-WMO global station (Italy, 2165 m a.s.l.). *Atmos. Chem. Phys.*, **13**, 15–30, https://doi.org/10.5194/acp-13-15-2013.

de Magalhães, N., H. Evangelista, T. Condom, A. Rabatel, and P. Ginot, 2019: Amazonian biomass burning enhances tropical Andean glaciers melting. *Sci. Rep.*, **9**, 16914, https://doi.org/10.1038/s41598-019-53284-1.

Deng, X., J. Chen, L. A. Hansson, X. Zhao, and P. Xie, 2021: Eco-chemical mechanisms govern phytoplankton emissions of dimethylsulfide in global surface waters. *Natl. Sci. Rev.*, **8**, nwaa140, https://doi.org/10.1093/nsr/nwaa140.

Deng, Y., and Coauthors, 2018: Hygroscopicity of organic aerosols and their contributions to CCN concentrations over a midlatitude forest in Japan. *J. Geophys. Res. Atmos.*, **123**, 9703–9723, https://doi.org/10.1029/2017JD027292.

Dunne, E. M., and Coauthors, 2016: Global atmospheric particle formation from CERN CLOUD measurements. *Science*, **354**, 1119–1124, https://doi.org/10.1126/science.aaf2649.

Falvey, M., and R. D. Garreaud, 2005: Moisture variability over the South American Altiplano during the South American low level jet experiment (SALLJEX) observing season. *J. Geophys. Res.*, **110**, D22105, https://doi.org/10.1029/2005JD006152.

Fiebig-Wittmaack, M., E. Schultz, A. M. Córdova, and C. Pizarro, 2006: A microscopic and chemical study of airborne coarse particles with particular reference to sea salt in Chile at 30°S. *Atmos. Environ.*, **40**, 3467–3478, https://doi.org/10.1016/j.atmosenv.2006.02.008.

Gatari, M. J., J. B. C. Pettersson, W. Kimani, and J. Boman, 2009: Inorganic and black carbon aerosol concentrations at a high altitude on Mt Kenya. *X-Ray Spectrom.*, **38**, 26–36, https://doi.org/10.1002/xrs.1094.

Gordon, H., and Coauthors, 2016: Reduced anthropogenic aerosol radiative forcing caused by biogenic new particle formation. *Proc. Natl. Acad. Sci. USA*, **113**, 12 053–12 058, https://doi.org/10.1073/pnas.1602360113.

Hamburger, T., and Coauthors, 2013: Long-term in situ observations of biomass burning aerosol at a high altitude station in Venezuela – Sources, impacts and interannual variability. *Atmos. Chem. Phys.*, **13**, 9837–9853, https://doi.org/10.5194/acp-13-9837-2013.

Henze, D. K., J. H. Seinfeld, N. L. Ng, J. H. Kroll, T. M. Fu, D. J. Jacob, and C. L. Heald, 2008: Global modeling of secondary organic aerosol formation from aromatic hydrocarbons: High- vs. low-yield pathways. *Atmos. Chem. Phys.*, **8**, 2405–2420, https://doi.org/10.5194/acp-8-2405-2008.

IPCC, 2013: *Climate Change 2013: The Physical Science Basis*. Cambridge University Press, 1535 pp., https://doi.org/10.1017/CBO9781107415324.

Ji, Y., and Coauthors, 2017: Reassessing the atmospheric oxidation mechanism of toluene. *Proc. Natl. Acad. Sci. USA*, **114**, 8169–8174, https://doi.org/10.1073/pnas.1705463114.

Kerminen, V. M., X. Chen, V. Vakkari, T. Petäjä, M. Kulmala, and F. Bianchi, 2018: Atmospheric new particle formation and growth: Review of field observations. *Environ. Res. Lett.*, **13**, 103003, https://doi.org/10.1088/1748-9326/aadf3c.

Kivekäs, N., and Coauthors, 2009: Long term particle size distribution measurements at Mount Waliguan, a high-altitude site in inland China. *Atmos. Chem. Phys.*, **9**, 5461–5474, https://doi.org/10.5194/acp-9-5461-2009.

Koenig, A. M., and Coauthors, 2021: Seasonal patterns of atmospheric mercury in tropical South America as inferred by a continuous total gaseous mercury record at Chacaltaya station (5240 m) in Bolivia. *Atmos. Chem, Phys.,* **21**, 3447–3472, https://doi.org/10.5194/acp-21-3447-2021.

Kulmala, M., 2018: Build a global Earth observatory. *Nature*, **553**, 21–23, https://doi.org/10.1038/d41586-017-08967-y.

Laj, P., and Coauthors, 2020: A global analysis of climate-relevant aerosol properties retrieved from the network of Global Atmosphere Watch (GAW) near-surface observatories. *Atmos. Meas. Tech.*, **13**, 4353–4392, https://doi.org/10.5194/amt-13-4353-2020.

Lenters, J. D., and K. H. Cook, 1997: On the origin of the Bolivian high and related circulation features of the South American climate. *J. Atmos. Sci.*, **54**, 656–678, https://doi.org/10.1175/1520-0469(1997)054<0656:OTOOTB>2.0.CO;2.

Li, C., N. A. Krotkov, P. J. T. Leonard, S. Carn, J. Joiner, R. J. D. Spurr, and A. Vasilkov, 2020: Version 2 Ozone Monitoring Instrument SO_2 product (OMSO2 V2): New anthropogenic SO_2 vertical column density dataset. *Atmos. Meas. Tech.*, **13**, 6175–6191, https://doi.org/10.5194/amt-13-6175-2020.

Mäkelä, J. M., M. Riihelä, A. Ukkonen, V. Jokinen, and J. Keskinen, 1996: Comparison of mobility equivalent diameter with Kelvin-Thomson diameter using ion mobility data. *J. Chem. Phys.*, **105**, 1562–1571, https://doi.org/10.1063/1.472017.

Merikanto, J., D. V. Spracklen, G. W. Mann, S. J. Pickering, and K. S. Carslaw, 2009: Impact of nucleation on global CCN. *Atmos. Chem. Phys.*, **9**, 8601–8616, https://doi.org/10.5194/acp-9-8601-2009.

Mohr, C., and Coauthors, 2019: Molecular identification of organic vapors driving atmospheric nanoparticle growth. *Nat. Commun.*, **10**, 4442, https://doi.org/10.1038/s41467-019-12473-2.

Molteni, U., F. Bianchi, F. Klein, I. El Haddad, C. Frege, M. J. Rossi, J. Dommen, and U. Baltensperger, 2018: Formation of highly oxygenated organic molecules from aromatic compounds. *Atmos. Chem. Phys.*, **18**, 1909–1921, https://doi.org/10.5194/acp-18-1909-2018.

Ng, N. L., M. R. Canagaratna, J. L. Jimenez, P. S. Chhabra, J. H. Seinfeld, and D. R. Worsnop, 2011: Changes in organic aerosol composition with aging inferred from aerosol mass spectra. *Atmos. Chem. Phys.*, **11**, 6465–6474, https://doi.org/10.5194/acp-11-6465-2011.

Osada, K., M. Kido, H. Iida, K. Matsunaga, Y. Iwasaka, M. Nagatani, and H. Nakada, 2003: Seasonal variation of free tropospheric aerosol particles at Mt. Tateyama, central Japan. *J. Geophys. Res.*, **108**, 8667, https://doi.org/10.1029/2003JD003544.

Pedregosa, F., and Coauthors, 2011: Scikit-Learn: Machine learning in Python. *J. Mach. Learn. Res.*, **12**, 2825–2830.

Perry, L. B., and Coauthors, 2017: Characteristics of precipitating storms in glacierized tropical Andean cordilleras of Peru and Bolivia. *Ann. Amer. Assoc. Geogr.*, **107**, 309–322, https://doi.org/10.1080/24694452.2016.1260439.

Rayner, N. A., D. E. Parker, E. B. Horton, C. K. Folland, L. V. Alexander, D. P. Rowell, E. C. Kent, and A. Kaplan, 2003: Global analyses of sea surface temperature, sea ice, and night marine air temperature since the late nineteenth century. *J. Geophys. Res.*, **108**, 4407, https://doi.org/10.1029/2002JD002670.

Reddington, C. L., and Coauthors, 2017: The Global Aerosol Synthesis and Science Project (GASSP): Measurements and modeling to reduce uncertainty. *Bull. Amer. Meteor. Soc.*, **98**, 1857–1877, https://doi.org/10.1175/BAMS-D-15-00317.1.

Rodríguez, S., Y. González, E. Cuevas, R. Ramos, P. M. Romero, J. Abreu-Afonso, and A. Redondas, 2009: Atmospheric nanoparticle observations in the low free troposphere during upward orographic flows at Izaña Mountain Observatory. *Atmos. Chem. Phys.*, **9**, 6319–6335, https://doi.org/10.5194/acp-9-6319-2009.

Rose, C., and Coauthors, 2015: Frequent nucleation events at the high altitude station of Chacaltaya (5240 m a.s.l.), Bolivia. *Atmos. Environ.*, **102**, 18–29, https://doi.org/10.1016/j.atmosenv.2014.11.015.

——, and Coauthors, 2017: CCN production by new particle formation in the free troposphere. *Atmos. Chem. Phys.*, **17**, 1529–1541, https://doi.org/10.5194/acp-17-1529-2017.

Schmeissner, T., and Coauthors, 2011: Analysis of number size distributions of tropical free tropospheric aerosol particles observed at Pico Espejo (4765 m a.s.l.), Venezuela. *Atmos. Chem. Phys.*, **11**, 3319–3332, https://doi.org/10.5194/acp-11-3319-2011.

Shank, L. M., and Coauthors, 2012: Organic matter and non-refractory aerosol over the remote Southeast Pacific: Oceanic and combustion sources. *Atmos. Chem. Phys.*, **12**, 557–576, https://doi.org/10.5194/acp-12-557-2012.

Skamarock, W. C., and J. B. Klemp, 2008: A time-split nonhydrostatic atmospheric model for weather research and forecasting applications. *J. Comput. Phys.*, **227**, 3465–3485, https://doi.org/10.1016/j.jcp.2007.01.037.

Steiner, G., T. Jokinen, H. Junninen, M. Sipilä, T. Petäjä, D. Worsnop, G. P. Reischl, and M. Kulmala, 2014: High-resolution mobility and mass spectrometry of negative ions produced in a ^{241}Am aerosol charger. *Aerosol Sci. Technol.*, **48**, 261–270, https://doi.org/10.1080/02786826.2013.870327.

Vuille, M., and Coauthors, 2018: Rapid decline of snow and ice in the tropical Andes – Impacts, uncertainties and challenges ahead. *Earth-Sci. Rev.*, **176**, 195–213, https://doi.org/10.1016/j.earscirev.2017.09.019.

Wiedensohler, A., and Coauthors, 2018: Black carbon emission and transport mechanisms to the free troposphere at the La Paz/El Alto (Bolivia) metropolitan area based on the Day of Census (2012). *Atmos. Environ.*, **194**, 158–169, https://doi.org/10.1016/j.atmosenv.2018.09.032.